Thermodynamics and Kinetics of a Folded-Folded′ Transition at Valine-9 of a GCN4-Like Leucine Zipper

D. André d'Avignon, G. Larry Bretthorst, Marilyn Emerson Holtzer, and Alfred Holtzer
Department of Chemistry, Washington University, St. Louis, Missouri 63130 USA

ABSTRACT Spin inversion transfer (SIT) NMR experiments are reported probing the thermodynamics and kinetics of interconversion of two folded forms of a GCN4-like leucine zipper near room temperature. The peptide is $^{13}C^{\alpha}$-labeled at position V9(*a*) and results are compared with prior findings for position L13(*e*). The SIT data are interpreted via a Bayesian analysis, yielding local values of T_{1a}, T_{1b}, k_{ab}, k_{ba}, and K_{eq} as functions of temperature for the transition $F_a^{V9} \rightleftarrows F_b^{V9}$ between locally folded dimeric forms. Equilibrium constants, determined from relative spin counts at spin equilibrium, agree well with the ratios k_{ab}/k_{ba} from the dynamic SIT experiments. Thermodynamic and kinetic parameters are similar for V9(*a*) and L13(*e*), but not the same, confirming that the molecular conformational population is not two-state. The energetic parameters determined for both sites are examined, yielding conclusions that apply to both and are robust to uncertainties in the preexponential factor (kT/h) of the Eyring equation. These conclusions are 1) the activation free energy is substantial, requiring a sparsely populated transition state; 2) the transition state's enthalpy far exceeds that of either F_a or F_b; 3) the transition state's entropy far exceeds that of F_a, but is comparable to that of F_b; 4) "Arrhenius kinetics" characterize the temperature dependence of both k_{ab} and k_{ba}, indicating that the temperatures of slow interconversion are not below that of the glass transition. Any postulated free energy surface for these coiled coils must satisfy these constraints.

INTRODUCTION

Two-stranded coiled coils—comprising two parallel, registered α-helices slightly supertwisted—are important models for addressing physical questions concerning protein folding (Lupas, 1996). The simplicity and linearity of the structure long since allowed the link between sequence and structure to be forged. The structure is based upon a pseudo-repeating heptad of amino acids, designated *abcdefg*, in which residues *a* and *d* are hydrophobes and *e* and *g* oppositely charged (Crick, 1953; McLachlan and Stewart, 1975). The resulting pattern of hydrophobic and electrostatic interactions drives the dimerization.

Among coiled coils, the GCN4 leucine zipper (called GCN4-lz here) has been especially thoroughly studied (O'Shea et al., 1989, 1991; Goodman and Kim, 1991; Kenar et al., 1995). In particular, we have employed a pseudo-wild-type version (called GCN4-lzK here) mutated at four sites: R1K, H18K, R25K, and R33K, and with 99% $^{13}C^{\alpha}$ labels placed at selected sites as NMR targets (Lovett et al., 1996; Holtzer et al., 1997; d'Avignon et al., 1998). The full sequence of GCN4-lzK is given below.

The latter strategy has revealed several features of the population of conformational states as GCN4-lzK is heated, suggesting that it comprises more than two states: 1) at a given site, separate resonances appear for folded and unfolded species, allowing determination of site-specific thermal unfolding curves, curves that are seen to differ from site to site; 2) at most (but not all) sites, separate resonances appear for more than one *folded* form, allowing investigation of the thermodynamics and kinetics of interconversion of these folded substates.

Thus far, detailed study of the interconversion of two such dimeric folded substates has been reported for only one site: L13(*e*) (d'Avignon et al., 1998). That study was carried out by spin inversion transfer (SIT) NMR, resulting in determination of the equilibrium constant and rate constants (both ways) as functions of temperature for the process: $F_a^{L13} \rightleftarrows F_b^{L13}$, wherein F_a^{L13} signifies an ensemble of dimers folded at L13(*e*) in the form that dominates at the lowest temperatures, and F_b^{L13} signifies the corresponding ensemble folded at L13(*e*) in the form that dominates at moderate temperatures. Information is not yet available on the precise structural difference between these two dimeric folded forms.

If the interconversion of these two folded forms is a molecule-wide process, then corresponding data, taken at another site, would provide the same values for the rate and equilibrium constants and therefore the same activation parameters. Here, we test this idea by SIT studies at V9(*a*), a site distinct from L13(*e*), but in the same heptad. Specifically, we employ in this study the GCN4-lzK sequence: Ac-KMKQLEDKVEELLSKNYKLENEVAKLKKLVGEK-Am, wherein each underlined residue—V9(*a*), L19(*d*), and G31(*b*)—bears a 99% $^{13}C^{\alpha}$ label. Thus, we report here on the corresponding local process: $F_a^{V9} \rightleftarrows F_b^{V9}$.

As will be seen, the results indicate that the thermodynamic and kinetic parameters characterizing the transition between folded forms at V9(*a*) are similar to, but distinct from, those obtained for the related transition at L13(*e*). Once again, this suggests that a simple two-state picture is

Received for publication 2 October 1998 and in final form 29 January 1999.

Address reprint requests to Alfred Holtzer, Department of Chemistry, Washington University Campus Box 1134, One Brookings Drive, St. Louis, MO 63130-4899. Tel.: 314-935-6572; Fax: 314-935-4481; E-mail: holtzer@wuchem.wustl.edu.

0006-3495/99/05/2752/08 $2.00

inadequate to describe the population of global molecular conformations in these coiled coils. Our data also allow certain conclusions to be drawn about the transition state ensemble for the interconversion, conclusions that apply to both sites.

MATERIALS AND METHODS

Synthesis, purification, and characterization of GCN4-lzK labeled at V9(*a*), L19(*d*), and G31(*b*)

Methods for solid-phase peptide synthesis, preparation of $^{13}C^{\alpha}$-labeled Fmoc-amino acids, and purification and characterization of the completed, end-capped GCN4-lzK peptides have been described earlier (Holtzer et al., 1995, 1997; Lovett et al., 1996).

The molar mass of the purified peptide with 99% $^{13}C^{\alpha}$ at positions V9(*a*), L19(*d*), and G31(*b*) was found to be 3947.6 Da (3947.5 Da, expected) by electrospray mass spectrometry. The purified peptide is >98% pure by reversed-phase high-performance liquid chromatography using a Vydac C18 column, as described earlier (d'Avignon et al., 1998). Its thermal CD unfolding profile is indistinguishable from that of the natural abundance and of other $^{13}C^{\alpha}$-labeled GCN4-lzK peptides (Lovett et al., 1996). Solution concentrations, in formality of peptide chains, were determined from absorbance at 275 nm using an extinction coefficient of 1.40 cm^{-1} M^{-1}.

$^{13}C^{\alpha}$-NMR

The equilibrium and spin inversion transfer (SIT) experiments employed solutions of the peptide chains at a formal concentration of 1.24 mM in $(NaCl)_{100}(NaPi)_{50}(D_2O)_{5514}(7.4)$, wherein we designate aqueous solvents by giving the formula of each solute species with its millimolarity as a subscript followed by the pH in parentheses. This millimolarity of D_2O corresponds to 10% (v/v). Thermal unfolding equilibria of GCN4-lzK are independent of the presence of D_2O up to 17% (Lovett et al., 1996; Holtzer et al., 1997). Reversed-phase HPLC before and after the SIT studies showed no changes in the peptide.

In the relevant room-temperature region, the relative equilibrium population of the two folded forms is independent of peptide concentration, and the population of unfolded form at V9(*a*) is small at the relatively high concentration of the SIT experiments (Lovett et al., 1996; Holtzer et al., 1997).

All $^{13}C^{\alpha}$-NMR data were collected as previously described with respect to spectrometer, probe, NMR-tube size, susceptibility plugs, field-frequency lock methods, chemical shift referencing, sample temperature control, and decoupling techniques (Lovett et al., 1996; Holtzer et al., 1997; d'Avignon et al., 1998).

Magnetization transfer data were generated for site V9(*a*) using methods differing only slightly from those used earlier for L13(*e*) (d'Avignon et al., 1998). For V9(*a*), data were obtained by successively 1) issuing a Gaussian π-pulse of 40 ms duration, with 15.64 ms full width at half height, and centered at the resonance frequency of $^{13}C^{\alpha}$ at position V9(*a*) in its F_a^{V9} folded form (the downfield, i.e., less shielded, resonance); 2) delaying by a variable interval (τ = 0–1.7 s); 3) interrogating via a 17.5-μs, broad-band $\pi/2$ pulse; 4) recording the free induction decay (FID), the time from interrogation to the succeeding π-pulse (relaxation recovery period) being 2.3 s. Corresponding inversion at the F_b^{V9} frequency (the upfield, i.e., more shielded, resonance) followed, with identical protocol. Approximately 1400 transients were recorded, with interleaving, among 16 separate delay times. Thus, at each temperature, 16 separate FIDs were measured after F_a^{V9} inversion and an additional 16 FIDs after F_b^{V9} inversion. Our SIT data base at each temperature comprises these 32 FIDs. Some measurements were made with a 30-ms inversion pulse, instead of 40-ms. The latter is more discriminating, but the former provides somewhat greater dynamic range. The resulting values of the kinetic parameters are indistinguishable.

An equilibrium ^{13}C-NMR spectrum, without signal inversion, was also obtained at each temperature using relaxation delays of 2.60 s between transients. Spin counts from the latter provide assessments of the relative equilibrium populations of F_a^{V9} and F_b^{V9}. The resulting, separately determined, equilibrium constants can be compared with the k_{ab}^{V9}/k_{ba}^{V9} ratios obtained from the SIT data.

Such SIT and equilibrium data were collected at five temperatures from 20.1 to 31.6°C. The total data collection time at each temperature is ~26 h.

Bayesian data analysis

In the SIT experiment, the time course of restoration of the equilibrium is governed by four constants: the respective spin-lattice relaxation times at F_a^{V9} and F_b^{V9} (T_{1a}^{V9} and T_{1b}^{V9}) and the rate constants for the forward (k_{ab}^{V9}) and reverse (k_{ba}^{V9}) conformational reactions $F_a^{V9} \rightleftarrows F_b^{V9}$. The modified Bloch differential equations appropriate to such a system and their solutions have long been known (McConnell, 1958; Rudin and Sauter, 1992). The form actually used here has been given earlier (d'Avignon et al., 1998).

The 32 FIDs for each temperature were subjected to joint Bayesian analysis, as characterized earlier (d'Avignon et al., 1998). This analysis produces the time course of longitudinal magnetization at each site (after inversion at each respective site) and the four rate constants. The method has already been described in detail (Bretthorst, 1990a–c, 1997).

RESULTS

Fig. 1 shows the relevant $^{13}C^{\alpha}$-NMR spectra at the various temperatures employed. Our principal concern here is the region of resonances of residue V9(*a*). The complete range of resonances for this residue is marked from 62 to 69 ppm, as established earlier (Lovett et al., 1996; Holtzer et al., 1997). Near room temperature, resonances for two folded forms at V9(*a*) appear: F_a^{V9} at 68 ppm, dominant at low temperature, and F_b^{V9} at 67.5 ppm, dominant at moderate temperature. The resolution of resonances for the two folded forms at V9(*a*) is noticeably less than seen for the L13(*e*) site studied earlier (d'Avignon et al., 1998). It is noteworthy that the dominant form at low temperature is downfield from the other at V9(*a*), just opposite to the case of L13(*e*) studied earlier (d'Avignon et al., 1998). In this temperature range, the population of unfolded forms (near 63 ppm) is quite small.

In the particular peptide investigated here, residues L19(*d*) and G31(*b*) are also labeled. Their resonances appear in the range 54–59 and 44–47 ppm, respectively. The L19(*d*) resonance is unusual in that only one folded form is evident (Lovett et al., 1996; Holtzer et al., 1997). The G31(*b*) resonance region shows evidence of two poorly resolved folded forms (45.6–47 ppm), and of a small amount of unfolded form (45.5 ppm). Although we are principally concerned here with the V9(*a*) resonance, the others are a helpful check, since they must, and do, stay constant during the spin manipulations constituting the SIT experiments.

The changes wrought in the spectra with time in the SIT experiment are very similar to those displayed earlier (d'Avignon et al., 1998) and are not shown. Fig. 2 shows normalized longitudinal magnetizations just before and just

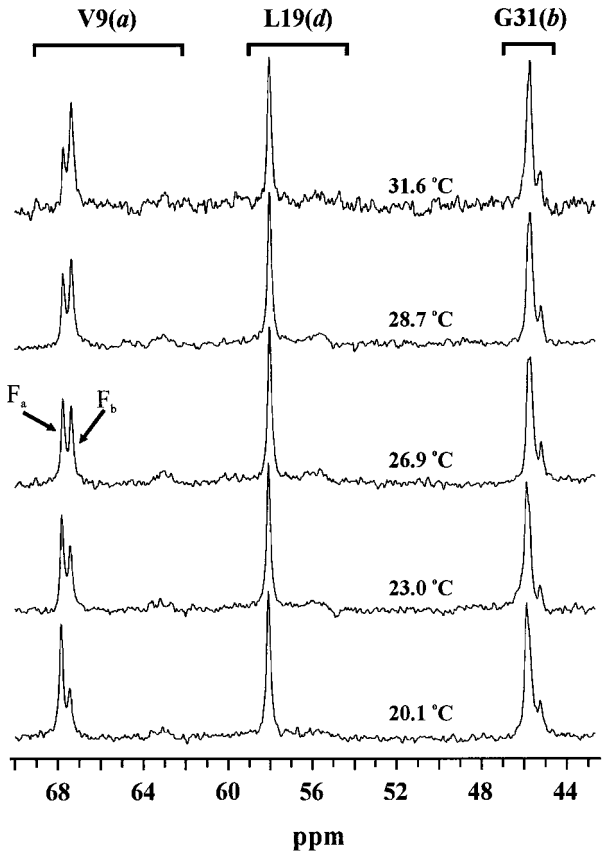

FIGURE 1 $^{13}C^{\alpha}$-NMR spectra of GCN4-lzK in $(NaCl)_{100}(NaPi)_{50}(D_2O)_{5514}$(7.4) near room temperature. Formal concentration of peptide chains, 1.24 mM. Regions for full range of resonances at the respective labeled sites V9(*a*), L19(*d*), and G31(*b*) are marked. V9(*a*) resonances assigned to local folded form favored at low T (F_a^{V9}) and at moderate T (F_b^{V9}) are also marked.

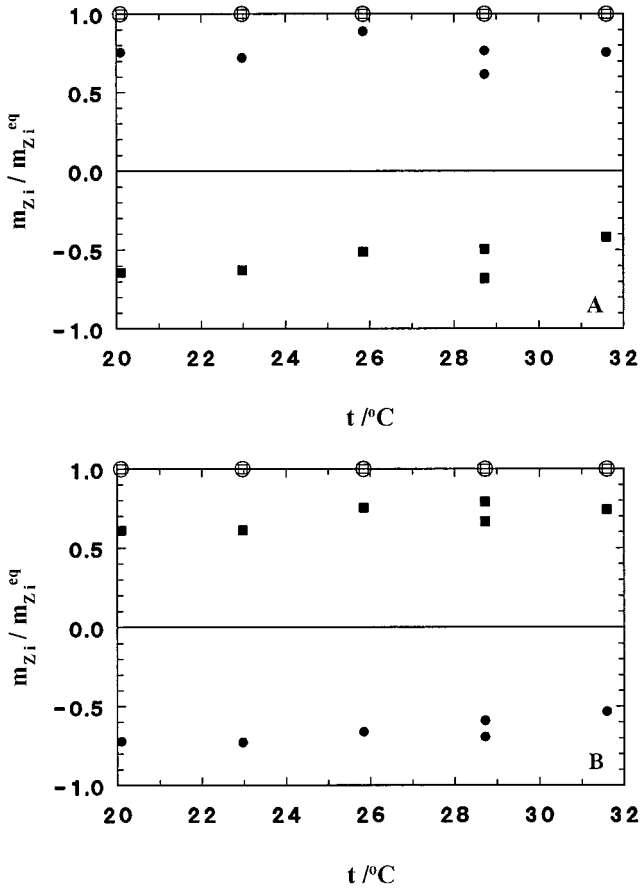

FIGURE 2 Effect of inversion pulse on longitudinal magnetization at V9(*a*) of GCN4-lzK. Solvent and peptide chain formality as in Fig. 1. All magnetizations first normalized to glycine (see text), then self-normalized to equilibrium values (see text). *Open symbols:* at equilibrium; *filled symbols:* at 0.0 s after Gaussian inversion centered at −0.020 s. *Squares:* values at F_a^{V9}; *circles:* values at F_b^{V9}. (*A*) F_a^{V9} inverted. (*B*) F_b^{V9} inverted.

after inversion at V9(*a*) and allows assessment of the efficiency of the Gaussian inversion pulse. To provide an internal amplitude reference, each magnetization was divided by the value for glycine (M_{ZG}) in the same spectrum, providing $m_{Za} = M_{Za}/M_{ZG}$ and $m_{Zb} = M_{Zb}/M_{ZG}$. These values were then self-normalized by dividing each by the equilibrium value m_{Zi}^{eq} at the same site. Thus, at spin equilibrium the ordinates at both sites are +1, and perfect inversion would change that to −1 at the inverted site, leaving the uninverted site unchanged. Fig. 2 *A* shows that the inversion at F_a^{V9} changes +1 to ~−0.4 to −0.6, depending very slightly on temperature. This average inversion is perhaps slightly less than seen for L13(*e*), but quite adequate to produce a substantial dynamic range in the recovery of spin equilibrium. In the same experiment (Fig. 2 *A*), the F_b^{V9} spin changes only slightly, from +1 to +0.8, independent of temperature.

If the initial inversion is at F_b^{V9} instead (Fig. 2 *B*), the performance is quite comparable. There, the ordinate change is a bit larger, from +1 to −0.5 to −0.7, again depending slightly on temperature. In Fig. 2 *B* the leakage of the inversion to the uninverted peak is almost the same as in Fig. 2 *A*. Since our data analysis makes no assumptions requiring perfection in the initial inversions, we conclude that, as in the case of L13(*e*), the inversion protocol provides a dynamic range appropriate for characterization of the time course of magnetization recovery.

Fig. 3 shows the temporal changes in magnetization intensities after inversion at each site at 28.7°C, along with the corresponding curves from the Bayesian analysis of the data. Evidently, Bayesian probability theory mimics the observations quite well in the case of the data for V9(*a*), as in the prior case of L13(*e*).

The Bayesian analysis yields the marginal posterior probabilities for the intrinsic spin-lattice relaxation times, T_{1a}^{V9} and T_{1b}^{V9}, and for the rate constants k_{ab}^{V9} and k_{ba}^{V9}. The T_1 values depend upon the molecular rotational correlation times, which are directly proportional to the medium's viscosity (η, which is temperature-dependent) and inversely proportional to the Kelvin temperature. In Fig. 4 the resulting T_1 values are plotted versus η/T. The positive slope of these plots, which is also evident in the case of L13(*e*), is expected for a molecule of the size of GCN4-lzK, whose

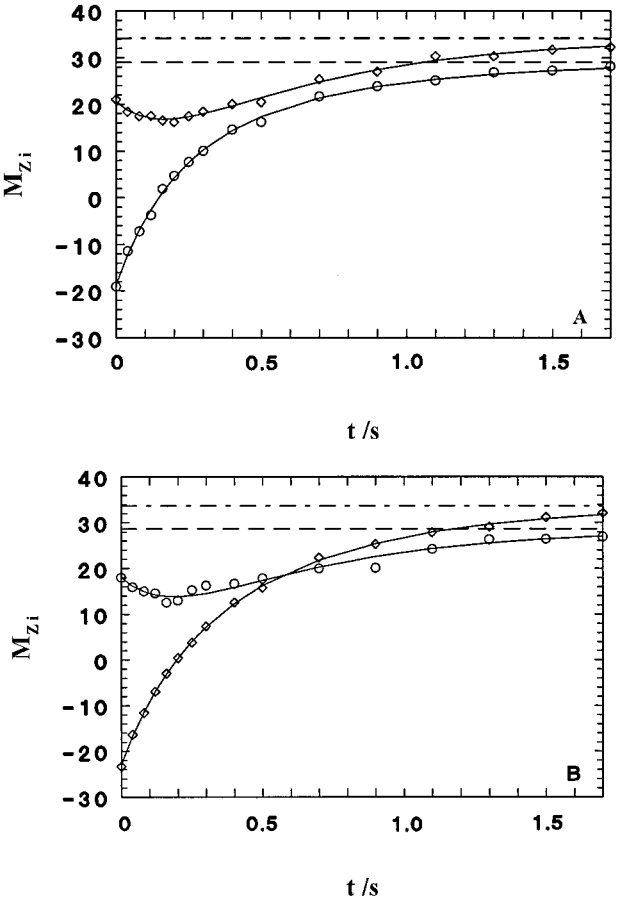

FIGURE 3 Time course of magnetization in SIT experiments for V9(*a*) of GCN4-lzK at 28.7°C. Solvent and peptide chain formality as in Fig. 1. *Open circles:* experimental F_a^{V9} magnetizations; *open diamonds:* experimental F_b^{V9} magnetizations. *Solid curves:* solutions to kinetic differential equations with parameters from Bayesian analysis. *Dashed horizontal lines:* calculated asymptotes for F_a^{V9} sites; *dot-dashed horizontal lines:* calculated asymptotes for F_b^{V9} sites. (*A*) F_a^{V9} inverted. (*B*) F_b^{V9} inverted.

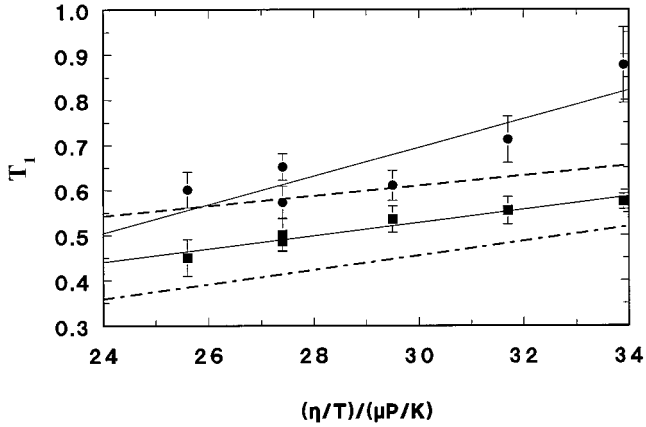

FIGURE 4 SIT-derived T_1 values at site V9(*a*) of GCN4-lzK versus $\eta(T)/T$. *Filled squares:* F_a^{V9}; *filled circles:* F_b^{V9}. Error bars are from Bayesian probability distributions. *Dot-dashed line:* prior result for F_a^{L13}; *dashed line:* prior result for F_b^{L13}.

rotational correlation time is likely appreciable. The numerical values of the spin-lattice relaxation times at residue V9(*a*) and the temperature dependence are quite similar to those for L13(*e*), except that the values of T_{1b}^{V9} show a slope that is about twice that of the others. It is not possible at present to interpret these T_1 values in physical terms. These relaxation times and other kinetic and thermodynamic constants determined from the Bayesian analysis of the data for V9(*a*) are summarized in Table 1.

Fig. 5 shows the relevant values from Table 1 as a van't Hoff plot. The equilibrium constants for the $F_a^{V9} \rightleftarrows F_b^{V9}$ reaction from spin equilibrium data (*open circles*) agree well with those from the ratio of the rate constants (k_{ab}/k_{ba}, *filled triangles*). The fit of the combined data to the van't Hoff equation, assuming constant enthalpy, is also shown (*solid line*). The agreement between the equilibrium values and the kinetically determined ones is slightly less exact than in the case of the data for residue L13(*e*) done earlier (d'Avignon et al., 1998). We ascribe this to the somewhat poorer resolution of the two resonances seen in V9(*a*) and/or the somewhat lower concentration employed. The different, but similar, line for the L13(*e*) case is shown for comparison.

Fig. 6 displays Arrhenius plots of the rate constants k_{ab}^{V9} (*open squares*) and k_{ba}^{V9} (*filled diamonds*), which are well fit by the Eyring equation (*solid lines*). Corresponding lines for the L13(*e*) site allow comparison. The relevant derived thermodynamic and kinetic parameters are shown in Table 2, along with previously determined values for site L13(*e*). It is apparent from Fig. 6 that the major difference between the two sites lies in the values of the forward rate constant, k_{ab}.

DISCUSSION

Correct interpretation of an experiment requires precise ideas about what is measured. We emphasize here again that the SIT-NMR technique refers to a particular site. Therefore, the reaction $F_a^{V9} \rightleftarrows F_b^{V9}$ signifies transition from an ensemble of dimers folded at V9 in the F_a conformation to the corresponding ensemble folded at the same site in the F_b conformation. In addition, it should be recognized that the SIT experiment manipulates nuclear spins only; the conformational equilibrium is left intact by the procedure. Thus, the rate constants determined refer to interconversion at equilibrium. It is, of course, a long-held principle that rate constants in idealute solutions are independent of whether the system is near or far from equilibrium, provided only that the reaction is not so fast as to cause the distribution of states to vary from thermal with time. There is no danger of this happening in protein conformational transitions.

Table 2 juxtaposes the thermodynamic and kinetic energetic parameters for position V9(*a*) with those obtained earlier for position L13(*e*). Fig. 7 summarizes this information pictorially. As can be seen, the general features of the transition are the same for both, but they differ in detail and the differences are outside the experimental errors. In particular, significant differences are seen in 1) the midpoint

TABLE 1 Thermodynamic and kinetic constants at V9(*a*) from $^{13}C^{\alpha}$-NMR

Temp. (°C)	T_{1a}/s*	T_{1b}/s*	k_{ab}/s^{-1}*	k_{ba}/s^{-1}*	k_{ab}/k_{ba}*	K_{eq}#
20.1	0.58 ± 0.02	0.88 ± 0.08	0.41 ± 0.03	0.88 ± 0.07	0.46 ± 0.01	0.41 ± 0.04
23.0	0.56 ± 0.03	0.71 ± 0.05	0.81 ± 0.06	1.21 ± 0.09	0.66 ± 0.01	0.59 ± 0.05
25.9	0.54 ± 0.03	0.61 ± 0.03	1.30 ± 0.07	1.46 ± 0.07	0.89 ± 0.01	0.81 ± 0.07
28.7	0.49 ± 0.02	0.65 ± 0.03	2.12 ± 0.09	1.80 ± 0.07	1.18 ± 0.01	1.21 ± 0.10
28.7	0.50 ± 0.04	0.57 ± 0.04	2.20 ± 0.12	1.85 ± 0.10	1.19 ± 0.02	1.21 ± 0.10
31.6	0.45 ± 0.04	0.60 ± 0.04	4.00 ± 0.23	2.63 ± 0.14	1.52 ± 0.02	1.62 ± 0.14

Values for $F_a^{V9} \rightleftarrows F_b^{V9}$ of GCN4-lzK in $(NaCl)_{100}(NaPi)_{50}(D_2O)_{5514}$ (7.4).
*From spin inversion transfer.
#From equilibrium magnetization intensities.

temperature for the transition ($\Delta T_m > 3$°C); 2) the standard enthalpies and entropies of the overall transition (from the combined fits of the equilibrium and SIT experiments); 3) the activation entropies in the forward reaction direction; 4) the activation enthalpies and entropies in the reverse reaction direction.

The existence of more than two resonances at a given site (Lovett et al., 1996) and the observed differences in thermal unfolding curves at different sites (Holtzer et al., 1997) leave little doubt that the global equilibrium conformational ensemble in GCN4-lzK comprises more than two states. The present finding that the thermodynamic and kinetic energetic parameters for interconversion between folded states also depend on chain position underscores that conclusion.

The geometrical relationship between the two sites is schematically shown in Fig. 8, which represents a molecular cross-section at the level of the heptad containing V9(*a*) and L13(*e*). It may seem remarkable that two sites within the same heptad could display such differences. This finding implies a rather rich array of conformational states. Additional evidence for this conclusion already exists in the substantial local differences seen in amide proton exchange rates in parent GCN4-lz (Goodman and Kim, 1991). The latter study also concludes that dynamics can be markedly different from site to site.

Although results for the transitions at V9(*a*) and L13(*e*) are not in quantitative agreement, they are qualitatively similar. The values in Table 2 and Fig. 7 thus should allow certain conclusions to be drawn that apply to both. With regard to the thermodynamic parameters for the overall transition, it is clear that the standard enthalpy change for the transition is substantial, 15–20 kcal/mol, perhaps as much as one-third of the value for complete unfolding of the analogous molecule of GCN4-lz, as measured by calorimetry (Kenar et al., 1995). We do not as yet have comparable calorimetric data for GCN4-lzK. The overall entropy change is also large, its contribution exactly compensating the enthalpy near room temperature, specifically 27.2°C at V9(*a*) and 24.0°C at L13(*e*).

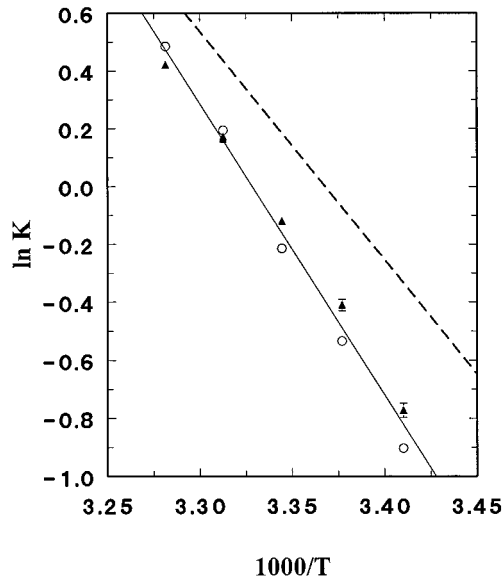

FIGURE 5 van't Hoff plot of equilibrium constants at site V9(*a*) of GCN4-lzK. *Open circles:* $[F_b^{V9}]/[F_a^{V9}]$ at spin equilibrium; *filled triangles:* k_{ab}^{V9}/k_{ba}^{V9} from SIT; *solid line:* least-squares combined fit. *Dashed line:* prior result for L13(*e*). Error bars appear only where error is larger than the symbol.

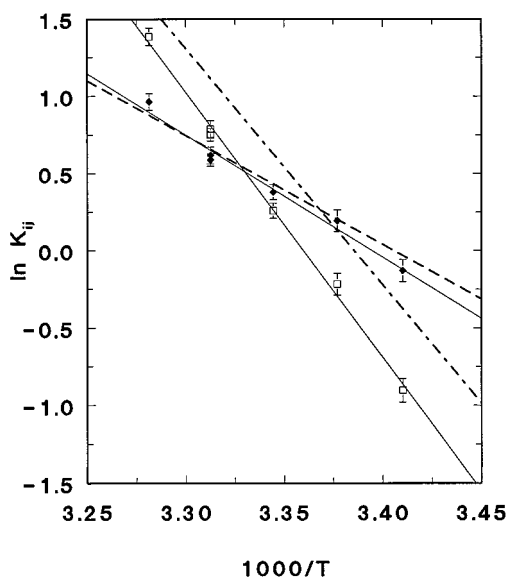

FIGURE 6 Arrhenius plots of rate constants for interconversion of folded forms at site V9(*a*) of GCN4-lzK. *Open squares:* k_{ab}^{V9}; *filled diamonds:* k_{ba}^{V9}; *solid lines:* least-squares fits to Eyring equation. *Dot-dashed line:* prior result for k_{ab}^{L13}; *dashed line:* prior result for k_{ba}^{L13}. Error bars appear only where error is larger than the symbol.

TABLE 2 Derived thermodynamic and kinetic parameters

	ΔG^{∞}*	$\Delta H^{\infty\#}$	$\Delta S^{\infty\S}$	$\Delta G^{\ddagger}_{ab,ba}$*	$\Delta H^{\ddagger\ \#}_{ab}$	$\Delta S^{\ddagger\ \S}_{ab}$	$\Delta H^{\ddagger\ \#}_{ba}$	$\Delta S^{\ddagger\ \S}_{ba}$
V9(*a*)	0.00 ± 0.03	20.0 ± 0.7	66.6 ± 2.5	17.28 ± 0.02	33.5 ± 1.0	54.0 ± 3.4	15.2 ± 1.0	−7.0 ± 3.4
L13(*e*)¶	0.00 ± 0.02	15.7 ± 0.6	52.8 ± 1.9	17.20 ± 0.01	29.8 ± 0.4	42.2 ± 1.4	13.5 ± 0.5	−12.7 ± 1.5

For $F_a \rightleftarrows F_b$ at V9(*a*) and at L13(*e*) of GCN4-lzK in $(NaCl)_{100}(NaPi)_{50}(D_2O)_{5514}$ (7.4).
*kcal/mol; interpolated to 27.2°C for V9(*a*) and to 24.0°C for L13(*e*), using van't Hoff (ΔG^{∞}) or Eyring ($\Delta G^{\ddagger}$) equation; for V9(*a*), ΔG^{∞} is from combined data fit of Fig. 5, and error estimates are from r.m.s. residuals in Fig. 5 (ΔG^{∞}) or 6 ($\Delta G^{\ddagger}_{ab,ba}$).
#kcal/mol; for V9(*a*), ΔH^{∞} from combined data fit of Fig. 5, with error estimates from standard least-squares analysis.
§cal/(K · mol); for V9*a*), ΔS^{∞} from combined data fit of Fig. 5, with error estimates from standard least-squares analysis.
¶All L13(*e*) values from d'Avignon et al., 1998.

Turning to kinetic characteristics, one must recognize that some of the kinetic values in Table 2 depend not only on the kinetic data, but on the Eyring equation, which was used to interpret them. This equation gives for the rate constant in either direction

$$k_{ab,ba} = \kappa(kT/h)\exp(-\Delta G_{ab,ba}{}^{\ddagger}/RT)$$
$$= \kappa(kT/h)\exp(\Delta S_{ab,ba}{}^{\ddagger}/R)\exp(-\Delta H_{ab,ba}{}^{\ddagger}/RT),$$

wherein κ is the transmission coefficient, k Boltzmann's constant, h Planck's constant, and R the gas constant. The transmission coefficient measures the probability that the reaction will pass through the transition state in the product direction along the reaction coordinate and go on to products, as opposed to retracing its trajectory back through the transition state in the opposite direction. The value of this parameter is rarely known in kinetic investigations and is generally assumed to be near unity. We will do so here, and the issue will not be further discussed below.

It is axiomatic that the chemical kinetics of a particular reaction is dictated by the free energy surface of the system, a multidimensional surface rarely known, even in crude approximation, to the investigator. In absence of such knowledge, a general theory that mimics major features of the physics is desirable, and the Eyring theory has gained broad acceptance for the purpose. It has been widely used for over half a century to interpret data in all branches of chemistry.

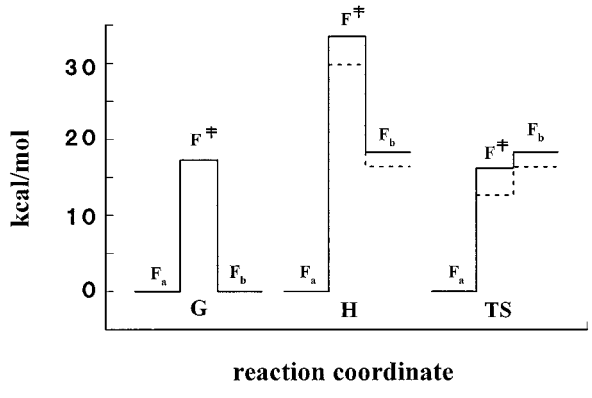

FIGURE 7 Schematic energy diagram at interpolated midpoint (27.2°C) of reaction $F_a^{V9} \rightleftarrows F_b^{V9}$. Double-dagger superscript designates transition state. From left to right, standard Gibbs energy, enthalpy, and temperature-entropy product, all from SIT. Abscissas (reaction coordinate) are shifted to allow parallel presentation. Ordinates (*G*, *H*, and *TS*) for form F_a^{V9} are arbitrarily set to zero. *Dashed lines:* prior results for L13 at its midpoint (24°C).

For reactions involving conformational changes of macromolecules, the uncertainties are compounded by both the vast phase space involved and the small secondary-bond energies connecting neighboring states. There is certainly no kinetic theory of such reactions that has gained general acceptance. Simulations have been useful, but invariably employ drastically reduced representations of the molecular structure and of the free-energy surface. Consequently, some workers have used Eyring theory in this context (Tan et al., 1996; d'Avignon et al., 1998), but others have not (Chan and Dill, 1997; Oliveberg et al., 1998; Laurents and Baldwin, 1998). Indeed, it is fair to say that none of the terms normally encountered in a kinetic investigation—e.g., "transition state," "reaction coordinate"—has a clear meaning where protein folding is concerned. Different investigators use different definitions (Chan and Dill, 1998; Du et al., 1998; Laurents and Baldwin, 1998; Nymeyer et al., 1998).

Criticisms of Eyring theory have generally focused on the preexponential factor kT/h, whose numerical value near room temperature is $\sim 6 \times 10^{12}\ s^{-1}$. Two grounds are usually presented for rejecting it. First, it is noted that the factor is often derived in the context of breaking an unstable covalent bond, and is therefore approximated as the inverse of the time for a single bond vibration, a derivation entirely inappropriate for protein folding transitions. Second, the Eyring theory is said to fail, because in the limit of zero Gibbs energy of activation, it requires the rate constant to be kT/h, i.e., of the order of $10^{12}\ s^{-1}$, which is numerically far greater than for the fastest possible protein folding process. The latter is generally agreed to be the helix-coil transition, whose rate constant is $\sim 10^{7}\ s^{-1}$.

Although we certainly agree that no general theory of protein folding is yet available, we find this verdict on Eyring theory to be overly harsh. The preexponential in Eyring theory is essentially the reciprocal of the mean lifetime of the transition state. As such, approximating it as kT/h can be justified by other means than through bond vibrations (Weston and Schwarz, 1972). The uncertainty principle requires that $\tau \Delta E \geq h$, wherein τ is the mean lifetime of the transition state and ΔE the uncertainty in its energy along the reaction coordinate. In Eyring theory, the transition state is considered to be in thermal equilibrium

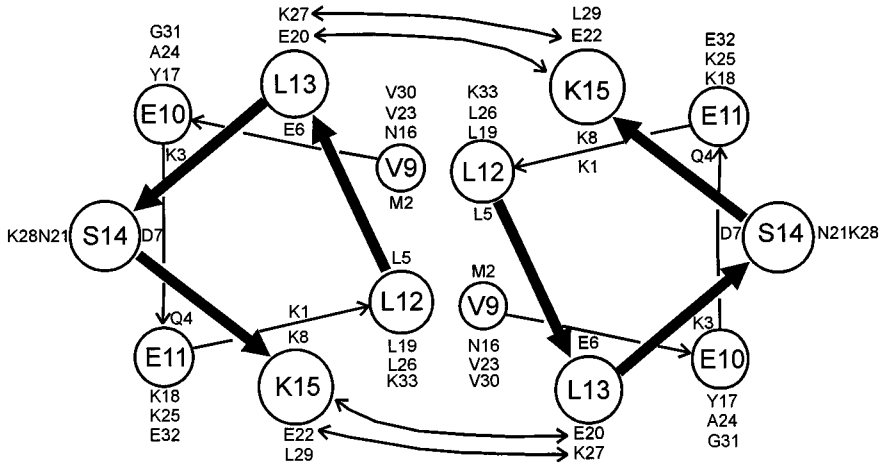

FIGURE 8 Schematic cross-section of the GCN4-lzK coiled coil at the level of residues 9–15, the heptad containing both V9(*a*) and L13(*e*). Helix direction is outward from the plane of the page. Residue types at corresponding sites in other heptads are also indicated. Double-headed arrows indicate canonical interhelical E20(*e*)-K15(*g*) and K27(*e*)-E22(*g*) salt bridges, which are seen in the x-ray crystal structure of parent GCN4-lz. The additional E6(*e*)-K1(*g*) interhelical salt bridges are canonical, but are not shown in the figure because the corresponding E6(*e*)-R1(*g*) bridges are not seen in the crystal structure of the parent.

with the system, and therefore ΔE must be something like the root-mean-square variance of the energy distribution in one dimension, i.e., of the order of kT. Therefore, $\tau \geq h/kT$. Furthermore, Eyring theory postulates that the transition state is a maximum along the reaction coordinate, i.e., inherently unstable. Hence, the lower limit for the lifetime can be selected, giving as a crude approximation $\tau = h/kT$, the same preexponential as before. Other derivations, more rigorous but less readily epitomized, yield the same result via arguments independent of bond vibrational considerations (Levine and Bernstein, 1987).

The second argument against Eyring theory is also questionable. The Eyring theory assumes that the transition state is an unstable state of free energy sufficiently large that it is sparsely populated, but a state that *must* be traversed (because it is the "least worst" way) to reach the reaction products. The entire theory rests on these assumptions and therefore on the proviso that $\Delta G^{\ddagger} \gg RT$. The Eyring equation therefore cannot be expected to reduce to the correct rate constant when the activation free energy is zero. The preexponential is of the order of the rate constant that would be observed, not if the activation free energy is zero, but if the entire molecular ensemble were to start in the transition state. This is not an experimentally accessible limit.

It is therefore not correct to say that Eyring theory gives a rate constant of kT/h when $\Delta G^{\ddagger} = 0$. The theory is, in fact, helpless in that regime. This limitation is perhaps more familiar in the case of bimolecular chemical reactions, where Eyring theory has also been quite successful, but certainly does not reduce to the Smoluchowski equation in the zero activation limit. It is easy to find cases wherein diffusion control leads to rate constants far below the 10^{12} s^{-1} limit given in the Eyring equation. Yet, Eyring theory has been highly useful in such reactions when considerable activation is required. One must remember that the preexponential in a collision theory is independent of the free energy surface, whereas in Eyring theory it is the offspring of that surface.

It thus appears that, if the transition state ensemble for protein conformational changes can be viewed as an unstable state of high free energy, then use of the Eyring equation may be justified. However, it is certainly not clear that even these minimalist requirements are met for protein folding. Consequently, it is necessary to inquire as to the effects of failure of the Eyring equation on our conclusions.

It should first be noted that the existence of T in the Eyring preexponential is essentially immaterial. The temperature dependence introduced by this linear term is negligible compared to the exponential dependence in the enthalpy term. Second, it is evident from the form of the Eyring expression that a change in the preexponential affects the values (as obtained from fitting data) of $\Delta G^{\ddagger}$ and $\Delta S^{\ddagger}$, but not $\Delta H^{\ddagger}$. In order to estimate the effect of failure of the Eyring equation, we therefore recalculated these values, changing the preexponential to 10^7 s^{-1}, mimicking the fastest process involved in folding. Since this new value is actually a measured rate constant, it includes both exponential and preexponential factors. It therefore represents a *lower* limit to the proper preexponential, just as kT/h represents an upper limit.

The results of the recalculation are very similar for both sites, V9(*a*) and L13(*e*), so they can be discussed together. The value of $\Delta G^{\ddagger}$ changes appreciably from 17 to 9.3 kcal/mol, but is still substantial. The entropy ascribed to the transition state is no longer 20% less, but rather 25% more, than that of F_b. However, the enthalpy of the transition state remains 70–90% higher than for H_b.

The following conclusions concerning the kinetics are therefore robust, surviving possible deficiencies in the Eyring equation.

1. At both sites, V9(*a*) and L13(*e*), the activation free energy is large enough so that the transition state ensemble is sparsely populated compared to both F_a and F_b, i.e., $\exp(-G_a/RT) \gg \exp(-G^{\ddagger}/RT) \ll \exp(-G_b/RT)$. It has already been noted that only one folded form is seen in the NMR spectrum for site L19(*d*). We do not as yet know whether this is because the two forms there happen to share the same chemical shift, or only one folded form exists there, or the local transition is so rapid there that only an average resonance position is observable.

2. The activation enthalpies in both directions are large, perhaps, in the case of the forward reaction direction, an appreciable fraction of the enthalpy of overall unfolding. Therefore, as seen in Fig. 7, the transition state ensemble has a mean enthalpy much higher than that of either F_a or F_b, i.e., $H_a \ll H^{\ddagger} \gg H_b$.
3. The entropy of activation for the forward reaction is quite substantial, but that of the reverse reaction is much smaller (perhaps even negative), hence the mean entropy of the transition state ensemble considerably exceeds F_a's, but is comparable to F_b's, i.e., $S_a \ll S^{\ddagger} \approx S_b$.
4. The good fit of the data to an exponential in the reciprocal of temperature ("Arrhenius kinetics") indicates that the slowness of these transitions definitely does not arise because the near-room-temperature regime is below the glass transition for this system.

These data thus allow a beginning to be made toward determination of some of the characteristics of the free energy surface of these two-stranded coiled coils, in particular the activation parameters for the transition between two folded forms at two different sites. Many current studies have similar aims for these and other proteins. It is perhaps worth mentioning that the methods employed here do not rely on assumptions concerning the effects of denaturants or of mutations on the kinetics, as do approaches confined to data at a single temperature. We feel strongly that conclusions are more certain when temperature is employed as an experimental variable, since then the activation enthalpy, at the very least, can be determined with a high degree of certainty.

It is legitimate to inquire about the generality of our findings. Might globular proteins also exhibit such local differences in overall unfolded fraction and even distinct, local, interconverting *folded* forms? At present, we cannot say for sure, but our surmise is that such conformational complexity will be found in some globular proteins as well, but will be more commonly seen in proteins with relatively simple topologies such as the two-stranded coiled coils. One must remember that the conclusion that a conformational population is two-state rests on the choice of a baseline for some physical property, a choice often made so as to exclude all but the most highly cooperative change. In that sense, the conclusion is as much a product of that choice as of the system itself.

Finally, it may be worth noting that the type of local interconversion of folded forms seen here occurs in the near-physiological range. It is possible, therefore, that the dynamics we observe are as significant for protein function as for folding per se.

Mass spectrometry was provided by the Washington University Mass Spectrometry Resource, a National Institutes of Health Research Resource (Grant P41RR0954). Synthesis of the peptide was carried out by Dr. Eva Lovett. Development of the Bayesian techniques employed here was supported by National Institutes of Health Grant NS-35912 and by a license agreement with Varian Associates. One of us (A.H.) acknowledges informative discussions on Eyring theory with Prof. Robert Yaris and the continuing aid of the Luftmensch Society.

REFERENCES

Bretthorst, G. L. 1990a. Bayesian analysis. I. Parameter estimation using quadrature NMR models. *J. Magn. Reson.* 88:533–551.

Bretthorst, G. L. 1990b. Bayesian analysis. II. Model selection. *J. Magn. Reson.* 88:552–570.

Bretthorst, G. L. 1990c. Bayesian analysis. III. Applications to NMR signal detection, model selection, and parameter estimation. *J. Magn. Reson.* 88:571–595.

Bretthorst, G. L. 1997. Bayesian analysis software package user guide. Pub. No. 87-190172-00. Rev. A0197, Varian Associates, Palo Alto, CA.

Chan H. S., and K. A. Dill. 1997. From Levinthal to pathways to funnels. *Nat. Struct. Biol.* 4:10–19.

Chan, H. S., and K. A. Dill. 1998. Protein folding in the landscape perspective: chevron plots and non-Arrhenius kinetics. *Proteins.* 30:2–33.

Crick, F. 1953. The Fourier transform of a coiled coil. *Acta Crystallogr.* 6:689–697.

d'Avignon, D. A., G. L. Bretthorst, M. E. Holtzer, and A. Holtzer. 1998. Site-specific thermodynamics and kinetics of a coiled-coil transition by spin inversion transfer NMR. *Biophys. J.* 74:3190–3197.

Du, R., V. S. Pande, A. Y. Grosberg, T. Tanaka, and E. S. Shakhnovich. 1998. On the transition coordinate for protein folding. *J. Chem. Phys.* 108:334–350.

Goodman, E. M., and P. S. Kim. 1991. Periodicity of amide proton exchange rates in a coiled-coil leucine zipper peptide. *Biochemistry.* 30:11615–11620.

Holtzer, M. E., D. L. Crimmins, and A. Holtzer. 1995. Structural stability of short subsequences of the tropomyosin chain. *Biopolymers.* 35: 125–136.

Holtzer, M. E., E. G. Lovett, D. A. d'Avignon, and A. Holtzer. 1997. Thermal unfolding in a GCN4-like leucine zipper: $^{13}C^{\alpha}$-NMR chemical shifts and local unfolding equilibria. *Biophys. J.* 73:1031–1041.

Kenar, K. T., B. Garcia-Moreno, and E. Freire. 1995. A calorimetric characterization of the salt dependence of the stability of the GCN4 leucine zipper. *Protein Sci.* 4:1934–1938.

Laurents, D. V., and R. L. Baldwin. 1998. Protein folding: matching theory and experiment. *Biophys. J.* 75:428–434.

Levine, R. D., and R. B. Bernstein. 1987. Molecular Reaction Dynamics and Chemical Reactivity. Oxford University Press, New York. 173–190.

Lovett, E. G., D. A. d'Avignon, M. E. Holtzer, E. H. Braswell, D. Zhu, and A. Holtzer. 1996. Observation via one-dimensional $^{13}C^{\alpha}$-NMR of local conformational substates in thermal unfolding equilibria of a synthetic analog of the GCN4 leucine zipper. *Proc. Natl. Acad. Sci. USA.* 93: 1781–1785.

Lupas, A. 1996. Coiled coils: new structures and new functions. *TIBS.* 21:375–382.

McConnell, H. M. 1958. Reaction rates by nuclear magnetic resonance. *J. Chem. Phys.* 28:430–431.

McLachlan, A. D., and M. Stewart. 1975. Tropomyosin coiled-coil interactions. Evidence for an unstaggered structure. *J. Mol. Biol.* 98:293–304.

Nymeyer, N., A. E. Garcia, and J. N. Onuchic. 1998. Folding funnels and frustration in off-lattice minimalist protein landscapes. *Proc. Natl. Acad. Sci. USA.* 95:5921–5928.

Oliveberg, M., Y-J. Tan, M. Silow, and A. R. Fersht. 1998. The changing nature of the protein transition state: implications for the shape of the free-energy profile for folding. *J. Mol. Biol.* 277:933–943.

O'Shea, E. K., J. D. Klemm, P. S. Kim, and T. Alber. 1991. X-ray structure of the GCN4 leucine zipper, a two-stranded, parallel coiled coil. *Science.* 254:539–544.

O'Shea, E. K., R. Rutkowski, and P. S. Kim. 1989. Evidence that the leucine zipper is a coiled coil. *Science.* 243:538–542.

Rudin, M., and A. Sauter. 1992. Measurement of reaction rates in vivo using magnetization transfer techniques. *In* NMR Basic Principles and Progress. P. Diehl, E. Fluck, H. Günther, R. Kosfeld, and J. Seelig, editors. 27:257–293.

Tan, Y-J., M. Oliveberg, and A. R. Fersht. 1996. Titration properties and thermodynamics of the transition state for folding: comparison of two-state and multi-state folding pathways. *J. Mol. Biol.* 264:377–389.

Weston, R. E., and H. A. Schwarz. 1972. Chemical Kinetics. Prentice-Hall, Englewood Cliffs, NJ.